\



Integer quantum Hall effect in Kekulé-patterned graphene

Yawar Mohammadi and Samira Bahrami

Citation: Chin. Phys. B, 2022, 31 (**1**): 017305. DOI: 10.1088/1674-1056/ac1b82
Journal homepage: http://cpb.iphy.ac.cn; http://iopscience.iop.org/cpb

What follows is a list of articles you may be interested in

Nonlinear photoncurrent in transition metal dichalcogenide with warping term under illuminating of light

Guo-Bao Zhu(朱国宝), Hui-Min Yang(杨慧敏, and Yun-Hai Zhang(张运海)
Chin. Phys. B, 2021, 30 (**3**): 037301. DOI: 10.1088/1674-1056/abc53c

Topology and ferroelectricity in group-V monolayers

Mutee Ur Rehman, Chenqiang Hua(华陈强), Yunhao Lu(陆赟豪)
Chin. Phys. B, 2020, 29 (**5**): 057304. DOI: 10.1088/1674-1056/ab81ff

Adsorptions of metal adatoms on graphene-like BC_3 and their rich electronic properties: A first-principles study

Pengfei Sui(隋鹏飞), Jiaqi Dai(戴佳琦), Yinchang Zhao(赵银昌), Zhenhong Dai(戴振宏)
Chin. Phys. B, 2018, 27 (**9**): 097311. DOI: 10.1088/1674-1056/27/9/097311

Quantum anomalous Hall effect in real materials

Jiayong Zhang(张加永), Bao Zhao(赵宝), Tong Zhou(周通), Zhongqin Yang(杨中芹)
Chin. Phys. B, 2016, 25 (**11**): 117308. DOI: 10.1088/1674-1056/25/11/117308

Transport properties of the topological Kondo insulator SmB_6 under the irradiation of light

Guo-Bao Zhu(朱国宝), Hui-Min Yang(杨慧敏)
Chin. Phys. B, 2016, 25 (**10**): 107303. DOI: 10.1088/1674-1056/25/10/107303

Integer quantum Hall effect in Kekulé-patterned graphene

Yawar Mohammadi[†] and Samira Bahrami

Department of Physics, Farhangian University, Tehran, Iran

(Received 16 March 2021; revised manuscript received 15 July 2021; accepted manuscript online 7 August 2021)

Y-shaped Kekulé bond textures in a honeycomb lattice on a graphene-copper superlattice have recently been experimentally revealed. In this paper, the effects of such a bond modulation on the transport coefficients of Kekulé-patterned graphene are investigated in the presence of a perpendicular magnetic field. Analytical expressions are derived for the Hall and longitudinal conductivities using the Kubo formula. It is found that the Y-shaped Kekulé bond texture lifts the valley degeneracy of all Landau levels except that of the zero mode, leading to additional plateaus in the Hall conductivity accompanied by a split of the corresponding peaks in the longitudinal conductivity. Consequently, the Hall conductivity is quantized as $\pm ne^2/h$ for $n = 2,4,6,8,10,\ldots$, excluding some plateaus that disappear due to the complete overlap of the Landau levels of different cones. These results also suggest that DC Hall conductivity measurements will allow us to determine the Kekulé bond texture amplitude.

Keywords: AAA-stacked trilayer graphene, integer quantum Hall effect, Kubo formula, Hall conductivity

PACS: 73.43.–f, 72.80.Vp **DOI:** 10.1088/1674-1056/ac1b82

1. Introduction

Space-modulated two-dimensional materials in which the lattice structure is modified by strain, twisting of the layers or the substrate, etc. are very interesting platforms for novel physical phenomena.[2–8] Recently, Gutiérrez *et al.*[9] have revealed Y-shaped Kekulé bond textures in a honeycomb lattice on a graphene-copper superlattice, in which one of the six carbon atoms in each superlattice unit cell has no copper atoms below it and acquires a shorter nearest-neighbor bond length. Gamayun *et al.*[10] have shown that such a bond texture locks the valley degree of freedom of the charge carriers to their direction of motion, resulting in the breaking of the valley degeneracy of graphene and the emergence of two species of massless Dirac fermion in Y-shaped Kekulé-patterned graphene.[10] Other works have explored the effects of Kekulé textures on graphene; Wu *et al.*[11] proposed a type of valley field-effect transistor made from Y-shaped Kekulé-patterned graphene and explored tuning the valley pseudo-magneto resistance via an electric field. Andrade *et al.*[12] studied the effects of uniaxial strain on the band structures of all types of Kekulé-distorted graphene. Further works have investigated[13,14] the effects of Kekulé textures on the electronic transport properties of Kekulé-distorted graphene, as well as the consequences of Kekulé distortion on the optical conductivity[15,16] and dynamical polarization of graphene.[17]

To date, most of the works on the topic of Y-shaped Kekulé-patterned graphene have studied its properties in the absence of a magnetic field. It is, however, interesting to explore the effects of a Y-shaped Kekulé bond texture on the magnetotransport properties. Moreover, the integer quantum Hall effect is one of the most intriguing properties of two-dimensional electron-gas systems, in which the Hall conductivity in a strong magnetic field is quantized in integer multiples of e^2/h.[18] This effect has been observed in graphene, but with a different quantization that arises from its chiral massless Dirac-like spectrum.[19–21] Recently, several groups have studied the effects of the stacking order on the integer quantum Hall quantization of multilayer graphene.[22–27] In this paper, we address the effects of the Y-shaped Kekulé bond texture on the quantum Hall transport properties of single-layer graphene. We derive an analytical expression for the Hall conductivity and find that the presence of the Y-shaped Kekulé bond texture lifts the valley degeneracy of all Landau levels except that of the zero Landau level; this behavior is described by the Atiyah–Singer index theorem.[28] This leads to a new type of anomalous quantum Hall conductivity quantized as $\sigma_{xy} = \nu e^2/h$ with $\nu = \pm 2, \pm 4, \pm 6, \pm 8, \ldots$. We also obtain an analytical expression for the longitudinal conductivity, which, along with the analytical expression for the Hall conductivity, can be used to evaluate the Hall and longitudinal resistivities and to explore the effects of the Kekulé bond texture on them.

The rest of this paper is organized as follows. In Section 2, we introduce the formalism used and obtain analytical expressions for the Hall and longitudinal conductivities. Section 3 is devoted to presenting the results and a discussion. Finally, in Section 4, we end the paper with a summary and conclusions.

2. Model and formulation

Figure 1(a) shows the lattice structure of a Y-type Kekulé-patterned graphene. According to the tight-binding model proposed by Gamayun *et al.*,[10] the low-energy Hamiltonian for

[†]Corresponding author. E-mail: y.mohammadi@cfu.ac.ir

© 2022 Chinese Physical Society and IOP Publishing Ltd

Kekulé-patterned graphene is given by

$$\boldsymbol{H} = \begin{pmatrix} v_{\mathrm{F}}\boldsymbol{p}\cdot\boldsymbol{\sigma} & \tilde{\Delta}\boldsymbol{Q}_{\nu} \\ \tilde{\Delta}^{*}\boldsymbol{Q}_{\nu}^{\dagger} & v_{\mathrm{F}}\boldsymbol{p}\cdot\boldsymbol{\sigma} \end{pmatrix}, \tag{1}$$

where v_{F} is the band velocity of pristine graphene, $\boldsymbol{p}=(p_x,p_y)$ is a two-dimensional momentum, and $\boldsymbol{\sigma}=(\sigma_x,\sigma_y)$ are Pauli matrices. Furthermore, $\tilde{\Delta}$ is the energy coupling amplitude originating from the Kekulé bond texture and $\boldsymbol{Q}_{\nu}=v_{\mathrm{F}}(\nu p_x-\mathrm{i}p_y)\boldsymbol{\sigma}_0$ is the Kekulé texture coupling between Dirac Hamiltonians, where $\boldsymbol{\sigma}_0$ is the identity matrix and $\nu=\pm$ denote two types of Y-shaped Kekulé texture.[10] For simplicity, we consider a real $\tilde{\Delta}=\Delta_0$ and $\nu=1$. Note that complex $\tilde{\Delta}$ and $\nu=-1$ are equivalent upon a unitary transformation. In this model, the effects of bond modulation have been taken into account via the Kekulé bond texture amplitude, Δ_0. Therefore, the effect of the bond modulation on the quantum Hall effect in Kekulé-patterned graphene can be examined by changing Δ_0.

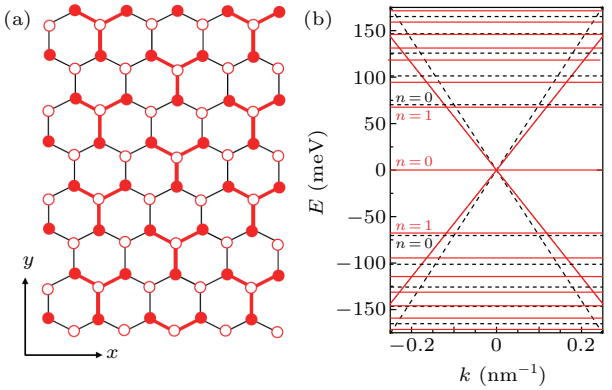


Fig. 1. (a) Schematic representation of a graphene Lattice with a Y-shaped Kekulé texture. Thick red and thin black lines distinguish different bond strengths. (b) The solid red (dashed black) curves show the low-energy spectrum of its slow(fast) cone with a velocity of $v_{\mathrm{F}}(1-\Delta_0)$ ($v_{\mathrm{F}}(1+\Delta_0)$) for a $\Delta_0=0.1$ Kekulé bond texture. The horizontal lines show the Landau levels for $B=4$ T.

2.1. Eigenvalues and eigenstates

The low-energy Hamiltonian of Kekule-patterned graphene in the presence of a perpendicular magnetic field is given by

$$\boldsymbol{H} = \begin{pmatrix} 0 & v_{\mathrm{F}}\pi_{-} & v_{\mathrm{F}}\Delta_0\pi_{-} & 0 \\ v_{\mathrm{F}}\pi_{+} & 0 & 0 & v_{\mathrm{F}}\Delta_0\pi_{-} \\ v_{\mathrm{F}}\Delta_0\pi_{+} & 0 & 0 & v_{\mathrm{F}}\pi_{-} \\ 0 & v_{\mathrm{F}}\Delta_0\pi_{+} & v_{\mathrm{F}}\pi_{+} & 0 \end{pmatrix}, \tag{2}$$

where $\pi_{\pm}=\pi_x\pm\mathrm{i}\pi_y$, $\boldsymbol{\pi}=-\mathrm{i}\hbar\nabla+e\boldsymbol{A}$ is the two-dimensional canonical momentum, and $\boldsymbol{A}$ is the vector potential. Due to the commutation relation $[\pi_{\pm},\pi_{\mp}]=\mp 2eB\hbar$, $\pi_{\pm}$ can be regarded as ascending and descending operators of the harmonic oscillators, $\pi\pm\rightarrow\sqrt{2}\hbar a^{\dagger}/l$ and $\pi\mp\rightarrow\sqrt{2}\hbar a/l$, where $l=\sqrt{\hbar/eB}$ is the magnetic length and the upper (lower) sign is for $\boldsymbol{B}=(0,0,B)$ ($\boldsymbol{B}=(0,0,-B)$). Assuming that the eigenfunctions are given by a linear combination of the eigenfunctions of the harmonic oscillator, we obtain the eigenvalues and eigenfunctions of Eq. (2) (except for the zero-energy eigenfunction) as follows. The eigenvalues are

$$E_n^{s_1,s_2} = \frac{\sqrt{2}\hbar v_{\mathrm{F}}}{l}\lambda_n^{s_1,s_2} \tag{3}$$

with

$$\lambda_n^{s_1,s_2} = s_2\sqrt{\frac{(2n+1)(1+\Delta_0^2)+s_1\sqrt{(1+\Delta_0^2)^2+16n(n+1)\Delta_0^2}}{2}}, \tag{4}$$

where $s_1=\pm$ denote the higher and lower subbands (called fast and slow cones) and $s_2=\pm$ denote the conduction and valence bands in the limit of the zero magnetic field, respectively. Figure 1(b) shows the Landau levels of Kekulé-patterned graphene for $\Delta_0=0.1$ and $B=4$ T. One can see that the Y-shaped Kekulé texture lifts the valley degeneracy, leading to the appearance of new Landau levels. For $n\geq 0$ and $\lambda_n^{s_1,s_2}\neq 0$, the eigenfunctions are given by

$$|n,s_1,s_2\rangle = \begin{bmatrix} \alpha_n^{s_1,s_2}|n-1\rangle \\ \beta_n^{s_1,s_2}|n\rangle \\ \gamma_n^{s_1,s_2}|n\rangle \\ \eta_n^{s_1,s_2}|n+1\rangle \end{bmatrix},$$

$$\begin{bmatrix} \alpha_n^{s_1,s_2} \\ \beta_n^{s_1,s_2} \\ \gamma_n^{s_1,s_2} \\ \eta_n^{s_1,s_2} \end{bmatrix} = \gamma_n^{s_1,s_2}\begin{bmatrix} \frac{\sqrt{n}}{\lambda_n^{s_1,s_2}}\frac{(\lambda_n^{s_1,s_2})^2-(n+1)(1-\Delta_0^2)}{(2n+1)\Delta_0} \\ \frac{(\lambda_n^{s_1,s_2})^2-(n+1)-n\Delta_0^2}{(2n+1)\Delta_0} \\ 1 \\ \frac{\sqrt{n+1}}{\lambda_n^{s_1,s_2}}\frac{(\lambda_n^{s_1,s_2})^2+n(1-\Delta_0^2)}{2n+1} \end{bmatrix}, \tag{5}$$

where

$$\gamma_n^{s_1,s_2} = \left[1+\left(\frac{(\lambda_n^{s_1,s_2})^2-(n+1)-n\Delta_0^2}{(2n+1)\Delta_0}\right)^2 + \left(\frac{\sqrt{n}}{\lambda_n^{s_1,s_2}}\frac{(\lambda_n^{s_1,s_2})^2-(n+1)(1-\Delta_0^2)}{(2n+1)\Delta_0}\right)^2 + \left(\frac{\sqrt{n+1}}{\lambda_n^{s_1,s_2}}\frac{(\lambda_n^{s_1,s_2})^2+n(1-\Delta_0^2)}{2n+1}\right)^2\right]^{-1/2}. \tag{6}$$

The zero-energy state ($\lambda_0^{-,s_2}=0$) is doubly degenerate; its eigenfunctions are given by

$$|0,-,+\rangle = \frac{1}{\sqrt{1+\Delta_0^2}}\begin{bmatrix} 0 \\ -|0\rangle \\ \Delta_0|0\rangle \\ 0 \end{bmatrix},$$

$$|0,-,-\rangle = \begin{bmatrix} 0 \\ 0 \\ 0 \\ |0\rangle \end{bmatrix}. \tag{7}$$

It is obvious that a nonzero Y-shaped Kekulé texture breaks the valley degeneracy of all Landau levels except those of the zero mode. As we show in the next section, this leads to a new type of anomalous quantum Hall effect, which is distinct from

that of pristine graphene.[19–21]

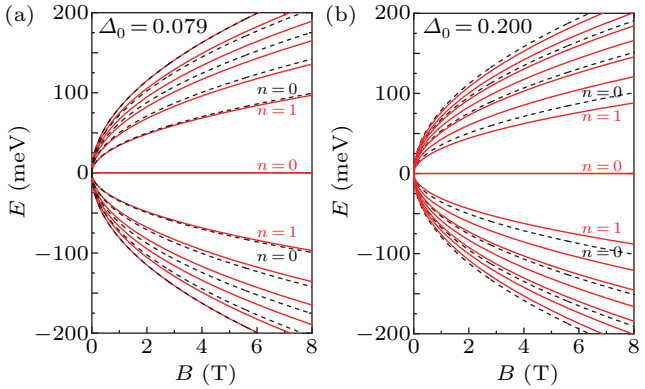


Fig. 2. Landau level spectrums of Y-shaped Kekulé-patterned graphene as a function of the perpendicular magnetic field for Kekulé bond texture amplitudes of (a) $\Delta_0 = 0.079$ and (b) $\Delta_0 = 0.200$.

Plots of the Landau level spectrums versus the magnetic fields for $\Delta_0 = 0.079$ and $\Delta_0 = 0.200$ are shown in Figs. 2(a) and 2(b), respectively. All the $E \neq 0$ Landau levels (including the $n = 0$ level of the fast cone with a velocity of $v_F(1+\Delta_0)$) scale according to $\sqrt{B}$ and nearly with $\sqrt{n}$. Due to the $\sqrt{n}$ dependence of the Landau levels, the separation between the adjacent Landau levels of each cone decreases with an increase in the index number of the Landau level. However, this is not the case for the separation between Landau levels of different cones. Consequently, some of the Landau levels of different cones overlap. For small Kekulé texture coupling amplitudes, this takes place at higher Landau levels. As we show in the results section, this can lead to the appearance of $8e^2/h$-steps and consequently the disappearance of the corresponding plateaus in the Hall conductivity.

2.2. Hall and longitudinal conductivity

In this subsection, we present our analytical results for the transverse (Hall) and longitudinal components of the conductivity tensors. In the linear response theory, the Hall conductivity is given by the Kubo formula[29–31]

$$\sigma_{xy} = \frac{\mathrm{i}\hbar e^2}{L_x L_y} \sum_{\zeta \neq \zeta'} \frac{f(E_\zeta) - f(E_{\zeta'})}{E_\zeta - E_{\zeta'}} \frac{\langle \zeta | v_y | \zeta' \rangle \langle \zeta' | v_x | \zeta \rangle}{E_\zeta - E_{\zeta'} + \mathrm{i}\Gamma}, \tag{8}$$

where $f(\varepsilon_\zeta) = 1/\left(1 + \mathrm{e}^{(E_\zeta - \mu)/k_\mathrm{B}T}\right)$ is the Fermi Dirac distribution function, μ is the chemical potential, $|\zeta\rangle$ are the eigenfunctions of Kekulé-patterned graphene in the Dirac notation given in the gauge $\boldsymbol{A} = (-By, 0, 0)$ by $\langle \boldsymbol{r} | n, s_1, s_2, k_x \rangle = \mathrm{e}^{\mathrm{i}k_x x} \mathrm{e}^{-z^2/2} H_n(z) / \sqrt{2^n n! \sqrt{\pi} l L_x}$ where $z = (y - k_x l^2)/l$, H_n is the Hermite polynomial, L_x (L_y) is the length of the graphene sheet in the x (y) direction, and finally, ε_ζ are the corresponding eigenvalues (Landau levels). Γ is the Landau level broadening due to the presence of disorders and other broadening mechanisms. However, for the real QHE, the Anderson localization due to impurity scattering is essential. In order to obtain an analytical result for σ_{xy} and estimate the possible step structures of σ_{xy}, we take $\Gamma = 0$. We will consider a finite broadening later, in the evaluation of the longitudinal conductivity.

To proceed, one needs the product of the velocity matrix elements. After evaluating and inserting them into Eq. (8), we arrive at

$$\begin{aligned}
\sigma_{xy} = & -\mathrm{sgn}(B) g_\sigma \frac{e^2}{h} \Bigg(+ \frac{1}{2} \sum_{s_2'} \left[f(E_0^{-,-}) - f(E_0^{+,s_2'}) \right] + \sum_{s_1', s_2'} \frac{(\alpha_n^{s_1', s_2'}(1 - \Delta_0^2))^2}{1 + \Delta_0^2} \frac{f(E_0^{-,+}) - f(E_1^{s_1', s_2'})}{(\lambda_0^{-,+} - \lambda_1^{s_1', s_2'})^2} \\
& + \sum_{s_2, s_1', s_2'} \left[\frac{\sqrt{2}\Delta_0}{\sqrt{1 + \Delta_0^2}} + \frac{s_2}{\sqrt{2}} (\Delta_0 \beta_1^{s_1'} + \gamma_{n', s'}) \right]^2 \frac{f(E_0^{+,s_2}) - f(E_1^{s_1', s_2'})}{(\lambda_0^{+,s_2} - \lambda_1^{s_1', s_2'})^2} \\
& + \sum_{n \geq 1} \sum_{s_1, s_2, s_1', s_2'} \left[(\beta_n^{s_1, s_2} + \Delta_0 \gamma_n^{s_1, s_2}) \alpha_{n+1}^{s_1', s_2'} + \eta_n^{s_1, s_2} \left(\Delta_0 \beta_{n+1}^{s_1', s_1'} + \gamma_{n+1}^{s_1', s_2'} \right) \right]^2 \frac{f(E_n^{s_1, s_2}) - f(E_{n+1}^{s_1', s_2'})}{(\lambda_n^{s_1, s_2} - \lambda_{n+1}^{s_1', s_2'})^2} \Bigg),
\end{aligned} \tag{9}$$

where $g_\sigma = 2$ is due to two-fold spin degeneracy (this is the case in which the Zeeman splitting is smaller than the Landau level broadening). After some cumbersome but straightforward calculations, the Hall conductivity can be written as

$$\sigma_{xy} = -\mathrm{sgn}(B) g_\sigma \frac{e^2}{h} \sum_{n \geq 0} \sum_{s_1, s_2} \tilde{f}(E_n^{s_1, s_2}), \tag{10}$$

where $\tilde{f}(E_n^{s_1, s_2}) = f(E_n^{s_1, s_2}) - 1/2$ is defined so that the formula continues to satisfy the particle–hole symmetry.[21,32] Equation (9) obviously indicates that σ_{xy} is an odd function of the chemical potential, $\sigma_{xy}(-\mu) = -\sigma_{xy}(\mu)$.

In a 2D electron system, a perpendicular magnetic field confines the electrons in quantized cyclotron orbitals. Therefore, at very low temperatures, the diffusive contribution to the conductivity vanishes and only its collisional (or hopping) part is nonzero.[33] The latter arises as a result of the migration of the cyclotron orbit due to electron–impurity scattering, which is assumed to play a key role in the transport properties of our system, as it is usual in other two-dimensional graphene-based materials. The longitudinal conductivity can therefore be writ-

ten as[29,30,33]

$$\sigma_{xx}^{\rm col} = \frac{e^2}{2k_{\rm B}TL_xL_y}\sum_{\zeta,\zeta'} f(E_\zeta)\left[1-f(E_{\zeta'})\right] \times W_{\zeta\zeta'}(E_\zeta,E_{\zeta'})(y_\zeta - y_{\zeta'})^2, \tag{11}$$

where $y_\zeta = \langle\zeta|y|\zeta\rangle$ and $W_{\zeta\zeta'}$ is the transition rate between the $|\zeta\rangle$ and $|\zeta'\rangle$ one-electron states. If the scattering due to impurities is assumed to be elastic, the transition rate is then given by[29,30,33]

$$W_{\zeta\zeta'}(E_\zeta,E_{\zeta'}) = \frac{2\pi n_{\rm i}}{\hbar L_xL_y}\sum_q |U(\boldsymbol{q})|^2|F_{\zeta\zeta'}(u)|^2 \times (E_\zeta - E_{\zeta'})\delta_{k_x,k_x'+q_x}, \tag{12}$$

where $n_{\rm i}$ is the impurity concentration, $F_{\zeta\zeta'}(u) = \langle\zeta|{\rm e}^{{\rm i}\boldsymbol{q}\cdot\boldsymbol{r}}|\zeta'\rangle$ is the form factor with $u = l^2q^2/2 = l^2(q_x^2+q_y^2)/2$, and $U(\boldsymbol{q})$ is the Fourier transform of the impurity potential, which is taken to be that of the screened charges, $U(\boldsymbol{r}) = e^2{\rm e}^{-k_{\rm s}r}/4\pi\varepsilon_{\rm r}\varepsilon_0 r$, in which $k_{\rm s}$ is the screening wave vector, $\varepsilon_{\rm r}$ is the relative permittivity, and ε_0 is the permittivity of vacuum. If the impurity potential is strongly short ranged, one may use the approximation $k_{\rm s} \gg q$ and ignore the q dependence of the Fourier transform of the impurity potential. Since the scattering is elastic and the eigenvalues do not depend on k_x, only the transitions $n \to n' = n$ are allowed. Furthermore, we have $(y_\zeta - y_{\zeta'})^2 = l^4q^2\cos^2\varphi$, where φ is the azimuthal angle in polar coordinates. Hence, transforming the sums into integrals

$$\sum_{k_x,\sigma} \to g_\sigma\frac{L_x}{4\pi^2l^2}\int_{-L_y/2l^2}^{L_y/2l^2}{\rm d}k_x,$$
$$\sum_q \to \frac{L_xL_y}{4\pi^2l^4}\int_0^{2\pi}{\rm d}\varphi\int_0^\infty {\rm d}u,$$

Eq. (11) takes the form

$$\sigma_{xy}^{\rm col} = g_\sigma\frac{e^2}{h}\frac{n_{\rm i}U_0^2}{2\sqrt{2}k_{\rm B}T\hbar v_{\rm F}lk_{\rm s}^2}\sum_{n,s_1,s_2} f(E_n^{s_1,s_2})\left[1-f(E_n^{s_1,s_2})\right] \times \int_0^\infty u\left|F_{n,n}^{s_1s_2,s_1s_2}(u)\right|^2{\rm d}u. \tag{13}$$

After evaluating the integral $\int_0^\infty u|F_{n,n}^{s_1s_2,s_1s_2}(u)|^2{\rm d}u$ analytically, using the orthogonality of the Laguerre polynomials and their recurrence relation,[34] we arrive at

$$\begin{aligned}\sigma_{xx} = g_\sigma\frac{e^2}{h}\frac{n_{\rm i}U_0^2}{2\sqrt{2}k_{\rm B}T\hbar v_{\rm F}lk_{\rm s}^2}\Bigg(&f(E_0^{-,-})\left[1-f(E_0^{-,-})\right] \\ &+f(E_0^{-,+})\left[1-f(E_0^{-,+})\right] \\ &+\frac{1}{2}\sum_{s_2}f(E_0^{+,s_2})\left[1-f(E_0^{+,s_2})\right] \\ &+\sum_{n\geq1}\sum_{s_1,s_2}\Big[(2n-1)(\alpha_n^{s_1,s_2})^2+\left[(\beta_n^{s_1,s_2})^2+(\gamma_n^{s_1,s_2})^2\right] \\ &\times\Big[(2n+1)\left((\beta_n^{s_1,s_2})^2+(\gamma_n^{s_1,s_2})^2\right)-2n(\alpha_n^{s_1,s_2})^2 \\ &-2(n+1)(\eta_n^{s_1,s_2})^2\Big]+(2n+3)(\eta_n^{s_1,s_2})^2\Big] \\ &\times f(E_n^{s_1,s_2})\left[1-f(E_n^{s_1,s_2})\right]\Bigg).\end{aligned} \tag{14}$$

This equation is numerically evaluated to obtain σ_{xx}. At very low temperatures, the effects of the other broadening mechanisms of the Landau levels can be taken into account by replacing $f(E_n^{s_1,s_2})\left[1-f(E_n^{s_1,s_2})\right]$ with an approximate Dirac delta function

$$\delta(E_n^{s_1,s_2}-\mu) \approx \frac{\Gamma/\pi}{(E_n^{s_1,s_2}-\mu)^2+\Gamma^2},$$

where Γ is the Landau level broadening.

3. Results and discussion

In this section, using the analytical expressions obtained in the previous section, the effects of the Y-shaped Kekulé bond texture on the transport coefficients of Kekulé-patterned graphene are investigated. In our calculation, we use the values $t = 3$ eV and $a = 0.142$ nm for the intra-layer hopping energy and the intra-layer carbon bond length of pristine graphene, respectively.

In Fig. 3, we plot the Hall and longitudinal conductivities of Y-shaped Kekulé-patterned graphene as a function of the chemical potential for fixed values of the magnetic field of $B = 7$ T, a temperature of $T = 5$ K, and a Y-shaped Kekulé bond texture of $\Delta_0 = 0.2$ (Fig. 3(b)), compared to those of pristine graphene (Fig. 3(a)). The other parameters are $n_{\rm i} = 5\times10^{13}$ m^{-2}, $\varepsilon_{\rm r} = 4$, and $k_{\rm s} = 5\times10^7$ nm^{-1}. In order to make the effects of the Kekulé bond texture more evident, we used a large value, $\Delta_0 = 0.2$, for it.[10] As is usual in the quantum Hall regime in two-dimensional materials, the Hall conductivity exhibits plateaus, and the transition regions between the plateaus of the Hall conductivity are accompanied by peaks in the longitudinal conductivity. Comparing Figs. 3(a) and 3(b) shows that in the presence of the Y-shaped Kekulé bond texture, additional plateaus appear (at $\pm ne^2/h$ for $n = 2,4,6,\ldots$) in the Hall conductivity of the Kekulé-patterned graphene, and that each peak of the longitudinal conductivity (except the peak located at a zero chemical potential) is split into two peaks.

The Hall plateaus displayed in Fig. 3 can be explained as follows. The Landau levels of pristine graphene are fourfold degenerate, so each Landau level contributes $4e^2/h$ to its Hall conductivity. On the other hand, as shown in Section 2, the Y-shaped Kekulé bond texture lifts the valley degeneracy of all Landau levels except that of the zero mode, which remains fourfold degenerate. So, each Landau level (except for the zero-energy level) contributes $2e^2/h$ ($4e^2/h$) to the Hall conductivity in Y-shaped Kekulé-patterned graphene, leading to the emergence of a $4e^2/h$-step at the zero chemical potential and $2e^2/h$-steps at other points in Fig. 3. Moreover, due to the

lifting of the valley degeneracy by the Y-shaped Kekulé bond distortion, each peak of the longitudinal conductivity (except the peak located at zero energy) is split into two peaks.

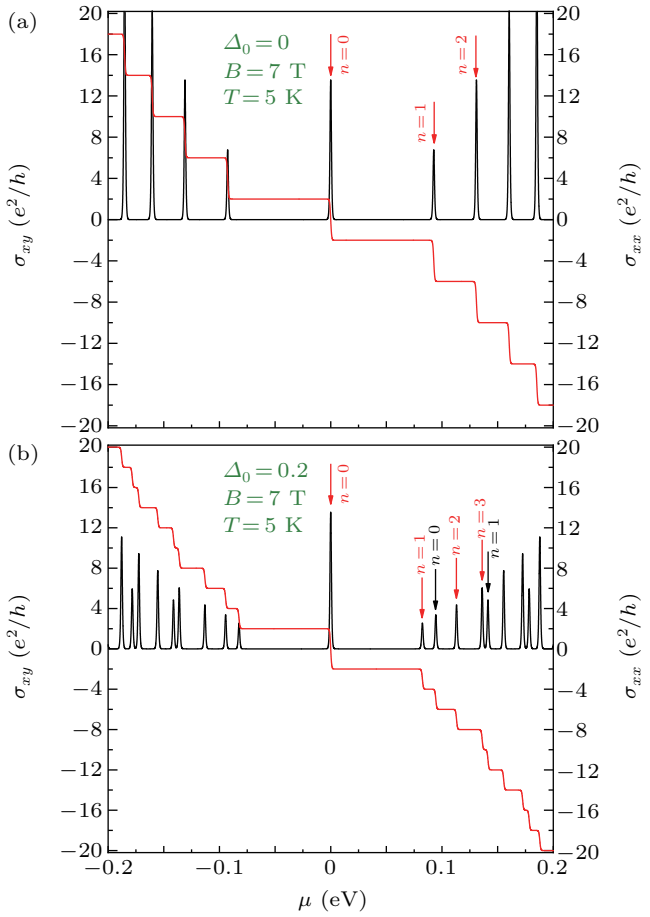


Fig. 3. The Hall and longitudinal conductivities of (a) pristine graphene and (b) Y-shaped Kekulé-patterned graphene for a Kekulé distortion of $\Delta_0 = 0.2$ versus the chemical potential. The other parameters are $B = 7$ T, $T = 5$ K, $n_i = 5 \times 10^{13}$ m^{-2}, $\varepsilon_r = 4$, and $k_s = 5 \times 10^7$ nm^{-1}.

As shown above, Y-shaped Kekulé-patterned graphene exhibits a new type of anomalous quantum Hall effect, which is distinct from that of pristine graphene.[19–21] The origin of the zero-energy Landau-level degeneracy and thus the anomalous quantum Hall effect in Kkeulé-patterned graphene, as in pristine single and bilayer graphene,[19,35,36] can be explained using the Atiyah–Singer index theorem.[28] According to this theorem, the existence of zero-energy states in curved lattices with identical topologies (e.g., for a corrugated graphene sheet with the same topology as that of a graphene lattice[37]) and/or in presence of a gauge field (the usual electromagnetic field provides just the simplest example of these fields), is guaranteed, for topological reasons. This means, in particular, that the number of zero-energy states expressed in terms of the total pseudo-magnetic/magnetic flux per torus in the units of the flux quantum is a topological invariant.[36,37] The number of zero-energy states can also be determined by the dimensions of the zero-energy eigenspaces.[37,38] For Kekulé-patterned graphene, if we decompose[10] $\boldsymbol{H} = \pi_+ \boldsymbol{S}_+ + \pi_- \boldsymbol{S}_-$, with $\boldsymbol{S}_\pm = v_F(\sigma_x \pm i\sigma_y) \otimes \tau_0 + v_F \Delta_0 \sigma_0 \otimes (\tau_x \pm i\tau_y)$ and $\boldsymbol{\sigma}_0$, $\boldsymbol{\sigma}_x$, and $\boldsymbol{\sigma}_y$ ($\boldsymbol{\tau}_0$, $\boldsymbol{\tau}_x$, and $\boldsymbol{\tau}_y$) act on the sublattice (valley) degree of freedom, we see that the full spaces of both $\boldsymbol{S}_+$ and $\boldsymbol{S}_-$ are composed of two irreducible rank-two null spaces, leading to a twofold degenerate zero mode for $\boldsymbol{H}$ and confirming the two-fold degeneracy of the zero-energy states. The degeneracy of the zero-energy states can be experimentally checked by measurements of the quantum Hall activation gaps of Kekulé-patterned graphene, similarly to Ref. [39] for the case of pristine single-layer graphene.

Due to the square-root dependence of the Landau levels on the applied magnetic field, the separation between the adjacent Landau levels of each cone decreases with an increase in the index number of the Landau level. However, this change in the distance between adjacent levels is not same for different cones. Consequently, the Landau levels of different cones can overlap. Moreover, according to Eqs. (3) and (4) and Fig. 2, the index numbers of the Landau levels that overlap with each other depend inversely on the Kekulé bond texture. Specifically, the lower the Kekulé texture coupling amplitude, the higher the Landau levels at which overlaps take place. The overlaps of the Landau levels lead to the emergence of $4e^2/h$-steps, and, consequently, the disappearance of the corresponding plateaus and peaks in the Hall and longitudinal conductivities, respectively. This takes place when the condition $\mu = E_n^{+,s_2} = E_m^{-,s_2}$, $m > n$ is satisfied for (m,n) pairs of indexes of the Landau levels of different cones. Based on this condition and Eq. (10), one may conclude that the plateaus that disappear are $-2s_2(n+m)e^2/h$. This effect can be seen in Fig. 4, in which we plot the Hall and longitudinal conductivities of Y-shaped Kekulé-patterned graphene as a function of the chemical potential for fixed values of the magnetic field ($B = 5$ T) and the temperature ($T = 3$ K) and different values of the Kekulé bond texture. One can see that this effect can be observed under a low magnetic field (chemical potential) if the Kekulé texture amplitude is large. A similar behavior, but with different step changes in the Hall conductivity, has been reported for AB-stacked bilayer graphene,[40] and bilayer[41] and trilayer[27] graphenes with an AA stacking order. However, unlike the bilayer[41] and trilayer[27] graphenes with an AA stacking order, the appearance of $4e^2/h$-steps in the Hall conductivity of Y-shaped Kekulé-patterned graphene and $8e^2/h$-steps in the Hall conductivity of AB-stacked bilayer graphene[40] is not periodical.

The Landau levels of pristine graphene, due to its linear band dispersion, are proportional to the square root of the indexes of the Landau levels. For this reason, the Landau levels close to the Dirac point are more widely spaced, allowing the quantum Hall effect ($\pm 2e^2/h$ plateaus in the Hall conductivity) to be observed under very magnetic field, even at room

temperature.[42] As one can see from Eqs. (10) and (11) and the plots of the Hall conductivity in Figs. 3 and 4, Y-shaped Kekulé-patterned graphene has fairly similar properties. The Hall conductivity, along with the $\sqrt{1+\Delta_0^2}$ dependence of the E_0^{+,s_2} Landau levels, may be used to measure the Y-shaped Kekulé bond texture amplitude.

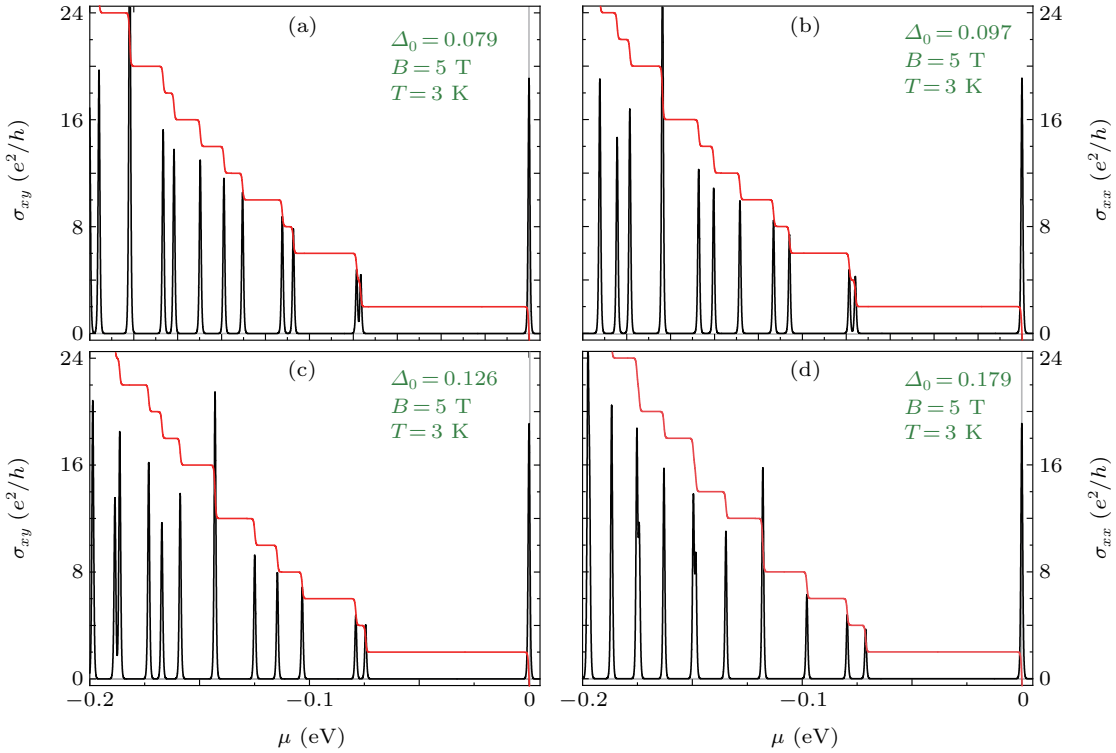


Fig. 4. The Hall and longitudinal conductivities of Y-shaped Kekulé-patterned graphene (lower panel) for amplitudes of (a) $\Delta_0 = 0.079$, (b) $\Delta_0 = 0.097$, (c) $\Delta_0 = 0.126$, and (d) $\Delta_0 = 0.179$ of the Kekulé bond texture versus the chemical potential. The appearance of $4e^2/h$-steps is evident.

Figure 5 shows (a) an energy spectrum of Kekulé-patterned graphene as a function of the magnetic field amplitude and (b) a counter plot of the quantized Hall conductivity of Kekulé-patterned graphene as functions of the energy and the magnetic field amplitude, for $\Delta_0 = 0.200$ and $T = 5$ K. In panel (b), the quantized values of the Hall conductivity inside the energy gaps are indicated by numbers. The sequence of the Hall conductivity, $\pm 2, \pm 4, \pm 6, \pm 8, \ldots$ in units of e^2/h is exactly half as large as that of pristine graphene (except for the first two filling factors), which originates from the twofold spin degeneracy (which, due to the spin and valley degeneracies, is equal to the Hall conductivity of pristine graphene). Furthermore, the plateau borders exhibit a $\sqrt{B}$ dependence that originates from the linear energy spectrum.

Figure 6 shows a Landau fan diagram[43–45] of (a) longitudinal conductivity and (b) Hall conductivity, in units of e^2/h, as a function of the magnetic field amplitude and the electron density. In Fig. 6, as in a conventional quantum Hall system, the Landau fan diagram exhibits straight lines that converge to the origin, tracking maxima in the longitudinal conductivity (Fig. 6(a)) and demarcating plateaus in the Hall conductivity (Fig. 6(b)). A Wannier diagram[46] has shown that the slope of each line of the longitudinal conductivity is precisely the Landau level filling factor, ν. Moreover, one can see that the peaks of the longitudinal conductivity broaden with increasing B, which is due to the broadening of the density of states.[31] On the other hand, with decreasing B, one sees numerous superficial peaks (at low electron densities) that gradually disappear when B vanishes. The reason for this is that for weak fields (B), the number of Landau levels near the Fermi level participating in the longitudinal conductivity increases.

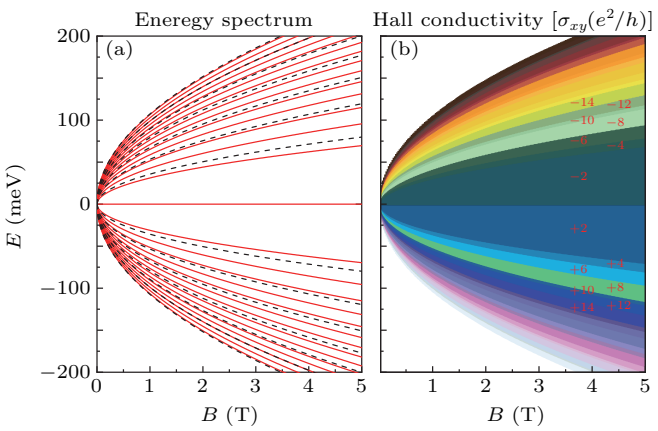


Fig. 5. (a) Energy spectrum of Kekulé-patterned graphene as a function of the magnetic field amplitude and the energy and (b) a counter plot of the quantized Hall conductivity of Kekulé-patterned graphene as functions of the energy and the magnetic field amplitude, for $\Delta_0 = 0.200$ and $T = 5$ K. In (b), the quantized values of the Hall conductivity inside the energy gaps are indicated by numbers. The Hall conductivity has been determined in the white areas.

Another notable feature of the fan diagram is that the number of peaks (and also the plateau borders) doubles for finite Δ_0, due to the lifting of the valley degeneracy.[31,44,45] Finally, it is worth mentioning that since, in this paper, the calculations are limited to low-energy electron transport, the fractal effects of Hofstadter butterfly spectra cannot be observed.

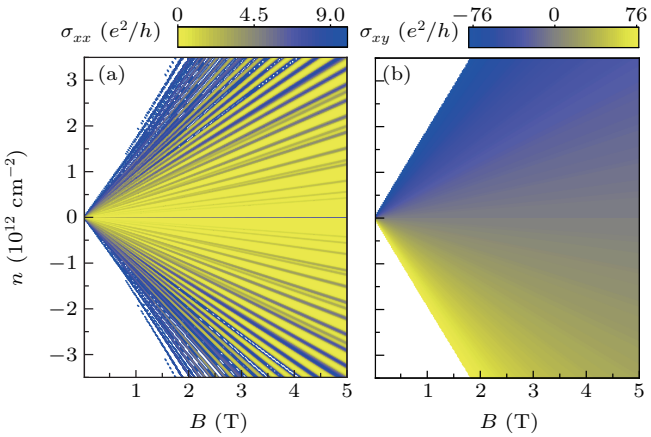


Fig. 6. Landau fan diagram of (a) longitudinal conductivity and (b) Hall conductivity, in units of e^2/h, as a function of the magnetic field amplitude and the electron density. The Hall and longitudinal conductivities have been determined in the white areas.

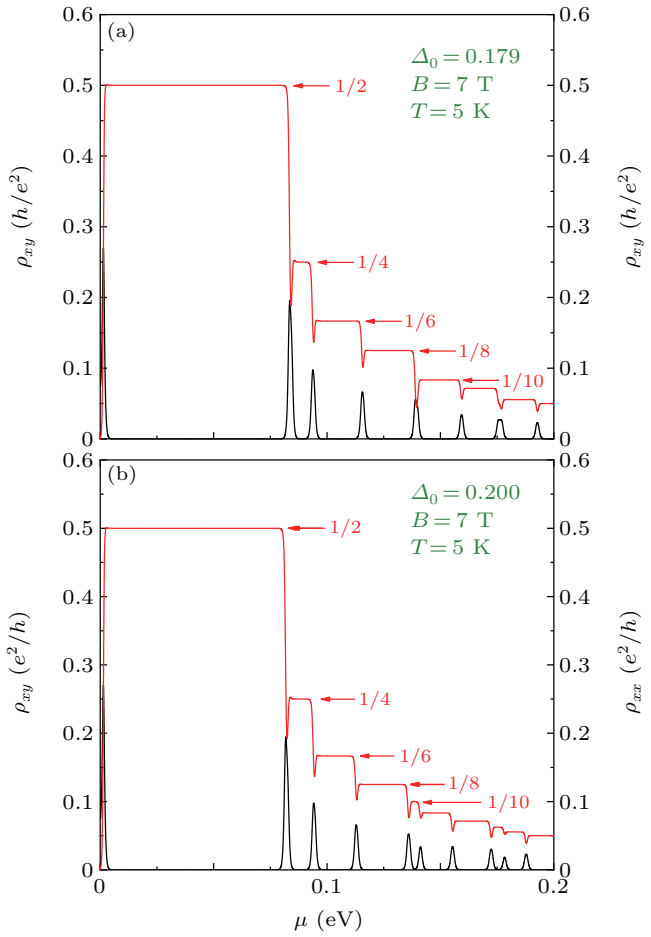


Fig. 7. The Hall and longitudinal resistivities of Y-shaped Kekulé-patterned graphene as a function of the charge carrier density for amplitudes of (a) $\Delta_0 = 0.179$ and (b) $\Delta_0 = 0.200$ of the Kekulé bond texture. The other parameters are $B = 7$ T, $T = 5$ K, $n_i = 5 \times 10^{13}$ m^{-2}, $\varepsilon_r = 4$, and $k_s = 5 \times 10^7$ nm^{-1}.

Most of the abovementioned effects can be observed in other measurable transport coefficients; for example, in the magnetoresistivity tensor whose components are written, in terms of the components of the conductivity tensor, as $\rho_{xx} = \rho_{yy} = \sigma_{xx}/(\sigma_{xx}\sigma_{yy} - \sigma_{xy}\sigma_{yx})$ and $\rho_{xy} = -\rho_{yx} = \sigma_{xy}/(\sigma_{xx}\sigma_{yy} - \sigma_{xy}\sigma_{yx})$, where $\sigma_{xx} = \sigma_{yy}$ and $\sigma_{yx} = -\sigma_{xy}$. Figure 7 displays the Hall and longitudinal resistivities of Y-shaped Kekulé-patterned graphene as a function of the chemical potential for amplitudes of (a) $\Delta_0 = 0.179$ and (b) $\Delta_0 = 0.200$ of the Kekulé bond texture. As expected, the Y-shaped Kekulé bond texture doubles the number of plateaus in the Hall resistivity (except for the first plateau), shown here at 1/2, 1/4, 16, 1/8, and so on, and splits the peaks of the longitudinal resistivity. The 1/10 plateau in the Hall resistivity (upper panel) disappears due to the overlap of the E_n^{+,s_2} and E_n^{+,s_2} Landau levels. Moreover, deep minimums occur in ρ_{xx} (strengthened at low chemical potential and when two Landau levels overlap), as shown when the longitudinal conductivity becomes large and/or exceeds the Hall conductivity. Similar deep minimums have been experimentally observed in graphene samples.[20,47]

4. Summary and conclusions

In summary, we investigated the effects of a Y-shaped Kekulé bond texture on the transport coefficients of a graphene superlattice in the presnce of a perpendicular magnetic field. It was shown that the Y-shaped Kekulé bond texture lifts the valley degeneracy of the Landau levels of pristine graphene (except for that of the zero mode), leading to the appearance of additional plateaus in the Hall conductivity of the Y-shaped Kekulé-patterned graphene and doubling the peaks of the Shubnikov–de Haas oscillations of the longitudinal conductivity. Moreover, it was found that the Hall conductivity in Y-shaped Kekulé-patterned graphene is quantized as $\sigma_{xy} = \nu e^2/h$ with filling factors of $\nu = \pm 2, \pm 4, \pm 6, \pm 8, \ldots$, except when two Landau levels from different cones overlap completely, which is satisfied when $\mu = E_n^{+,s_2} = E_m^{-,s_2}$, $m > n$. Complete overlap leads to the appearance of additional $4e^2/h$-steps and the simultaneous absence of $-2s_2(n+m)e^2/h$ plateaus, where pairs of integers (m,n) denote the indexes of the Landau levels that overlap, and $s_2 = +\ (-)$ denotes the conduction (valence) band of the fast cone. The effects of the Y-shaped Kekulé bond texture on the components of the magnetoresistivity tensor were also explored. Finally, the potential of the widely spaced $\pm 2e^2/h$ plateaus to be used in measuring the amplitude of the Y-shaped Kekulé bond texture was discussed.

Acknowledgement

Project supported by the Farhangian University.

References

[1] Chen G, Jiang L, Wu S, Lyu B, Li H, Chittari B L, Watanabe K, Taniguchi T, Shi Z, Jung J, Zhang Y and Wang F 2019 *Nat. Phys.* **15** 237.

[2] Yankowitz M, Jung J, Laksono E, Leconte N, Chittari B L, Watanabe K, Taniguchi T, Adam S, Graf D and Dean C R 2018 *Nature* **557** 404 .

[3] Cao Y, Fatemi V, Fang S., Watanabe K, Taniguchi T, Kaxiras E and Jarillo-Herrero P 2018 *Nature* **556** 43

[4] Naumis G G, Barraza-Lopez S, Oliva-Leyva M and Terrones H 2017 *Rep. Prog. Phys.* **80** 096501

[5] Chowdhury T, Kim J, Sadler E C, Li C, Lee S W, Jo K, Xu W N, Gracias D H, Drichko N V, Jariwala D, Brintlinger T H, Mueller T, Park H G and Kempa T J 2020 *Nat. Nanotechnol.* **15** 29

[6] Zhang D-B, Seifert G and Chang K 2014 *Phys. Rev. Lett.* **112** 096805

[7] Zhao J, Zhang G Y and Shi D X 2013 *Chin. Phys. B* **22** 057701

[8] Chu Y, Liu L, Yuan Y, Shen C, Yang R, Shi D, Yang W and Zhang G 2020 *Chin. Phys. B* **29** 128104

[9] Gutiérrez C, Kim C J, Brown L, Schiros T, Nordlund D, Lochocki E B, Shen K M, Park J and Pasupathy A N 2016 *Nat. Phys.* **12** 950

[10] Gamayun O V, Ostroukh V P, Gnezdilov N V, Adagideli İ and Beenakker C W J 2018 *New J. Phys.* **20** 023016

[11] Wu Q P, Chang L L, Li Y Z, Liu Z F and Xiao X B 2020 *Nanoscale Research Letters* **15** 1

[12] Andrade E, Carrillo-Bastos R and Naumis G G 2019 *Phys. Rev. B* **99** 035411

[13] Andrade E, Carrillo-Bastos R, Pantaleón P A and Mireles F 2020 *J. Appl. Phys.* **127** 054304

[14] Wang J J, Liu S, Wang J and Liu J F 2018 *Phys. Rev. B* **98** 195436

[15] Herrera S A and Naumis G G 2020 *Phys. Rev. B* **101** 205413

[16] Mohammadi Y 2021 *ECS J. Solid State Sci. Technol.* **10** 061011

[17] Herrera S A and Naumis G G 2020 *Phys. Rev. B* **102** 205429

[18] Klitzing K V, Dorda G and Pepper M 1980 *Phys. Rev. Lett.* **45** 494

[19] Novoselov K S, Geim A K, Morozov S V, Jiang D, Katsnelson M I, Grigorieva I V, Dubonos S V and Firsov A A 2005 *Nature* **438** 197

[20] Zhang Y, Tan Y W, Stormer H L and Kim P 2005 *Nature* **438** 201

[21] Gusynin V P and Sharapov S G 2005 *Phys. Rev. Lett.* **95** 146801

[22] McCann E and Fal'ko V I 2006 *Phys. Rev. Lett.* **96** 086805

[23] Henriksen E A, Nandi D and Eisenstein J P 2012 *Phys. Rev. X* **2** 011004

[24] Min H and MacDonald A H 2008 *Phys. Rev. B* **77** 155416

[25] Min H and MacDonald A H 2008 *Prog. Thror. Phys. Supp.* **176** 227

[26] Koshino M and Ando T 2008 *Phys. Rev. B* **77** 115313

[27] Mohammadi Y 2021 *Physica B* **613** 413022

[28] Atiyah M F and Singer I M 1968 *Ann. Math.* **87** 484

[29] Charbonneau M, Van Vliet K M and Vasilopoulos P 1982 *J. Math. Phys.* **23** 318

[30] Krstajić P M and Vasilopoulos P 2012 *Phys. Rev. B* **86** 115432

[31] Shakouri K H, Vasilopoulos P, Vargiamidis V and Peeters F M 2014 *Phys. Rev. B* **90** 235423

[32] Gusynin V P and Sharapov S G 2006 *Phys. Rev. B* **73** 245411

[33] Tahir M, Vasilopoulos P and Peeters F M 2015 *Phys. Rev. B* **92** 045420

[34] Tahir M and Vasilopoulos P 2015 *J. Phys.: Condens. Matter* **27** 075303

[35] Katsnelson M I 2007 *Mater. Today* **10** 20

[36] Katsnelson M I and Prokhorova M F 2008 *Phys. Rev. B* **77** 205424

[37] Pachos J K and Stone M 2007 *Int. J. Mod. Phys. B* **21** 5113

[38] Katsnelson M I 2020 *The Physics of Graphene* (Cambridge University Press) pp. 32–33

[39] Giesbers A J M, Zeitler U, Katsnelson M I, Ponomarenko L A, Mohiuddin T M and Maan J C 2007 *Phys. Rev. Lett.* **99** 206803

[40] Nakamura M, Hirasawa L and Imura K I 2008 *Phys. Rev. B* **78** 033403

[41] Hsu Y F and Guo G Y 2011 *Phys. Rev. B* **82** 165404

[42] Novoselov K S, Jiang Z, Zhang Y, Morozov S V, Stormer H L, Zeitler U, Maan J C, Boebinger G S, Kim P and Geim A K 2007 *Science* **315** 1379

[43] Dean C R, Wang L, Maher P, Forsythe C, Ghahari F, Gao Y, Katoch J, Ishigami M, Moon P, Koshino M, Taniguchi T, Watanabe K, Shepard K L, Hone J and Kim P 2013 *Nature* **497** 598.

[44] Chen G, Sui M, Wang D, Wang S, Jeil Jung J, Moon P, Shaffique Adam,Kenji Watanabe K, Taniguchi T, Shuyun Zhou S, Koshino M, Zhang G and Zhang Y 2017 *Nano Lett.* **17** 3576

[45] Yang W, Lu X, Chen G, Wu S, Xie G, Cheng M, Wang D, Yang R, Shi D, Watanabe K, Taniguchi T, Voisin C, Plaçais B, Zhang Y and Zhang G 2016 *Nano Lett.* **16** 2387

[46] Wannier G H 1978 *Phys. Status Solidi B* **88** 757

[47] Dean C R, Young A F, Cadden-Zimansky P, Wang L, Ren H, Watanabe K, Taniguchi T, Kim P, Hone J and Shepard K L 2011 *Nat. Phys.* **7** 693